LDA + DMFT study of the effects of correlation in LiFeAs

Johannes Ferber,* Kateryna Foyevtsova, Roser Valentí, and Harald O. Jeschke
Institut für Theoretische Physik, Goethe-Universität Frankfurt, Max-von-Laue-Strasse 1, D-60438 Frankfurt, Germany
(Received 7 November 2011; published 6 March 2012)

We discuss the role of electronic correlations in the iron-based superconductor LiFeAs by studying the effects on band structure, mass enhancements, and Fermi surface in the framework of density functional theory combined with dynamical mean field theory calculations. We conclude that LiFeAs shows characteristics of a moderately correlated metal and that the strength of correlations is mainly controlled by the value of the Hund's rule coupling J. The hole pockets of the Fermi surface show a distinctive change in form and size with implications for the nesting properties. Our calculations are in good agreement with recent angle-resolved photoemission spectroscopy and de Haas-van Alphen experiments.

DOI: 10.1103/PhysRevB.85.094505 PACS number(s): 71.27.+a, 74.20.Pq, 74.70.Xa, 71.18.+y

I. INTRODUCTION

High-temperature iron-based superconductors have been intensively studied since their discovery four years ago.[1] Among the various known iron pnictide classes, the 111 family comprising LiFeAs and LiFeP shows especially interesting features compared to the other families. Whereas superconductivity in many iron pnictide compounds develops in the vicinity of a spin-density-wave (SDW) state upon doping or application of external pressure, LiFeAs and LiFeP (and LaFePO from the 1111 family) are nonmagnetic and superconductivity evolves without additional doping or applied pressure. Of special relevance is LiFeAs where $T_c \approx 18$ K,[2,3] compared to LiFeP where $T_c \approx 6$ K[4] and LaFePO where $T_c \approx 4$ K.[5] In the 1111 and 122 family compounds (with LaFeAsO and $BaFe_2As_2$ as typical examples), the SDW order is generally attributed to sizable nesting of the electron and hole Fermi pockets.[6] For LiFeAs, the situation is not quite as clear: band structure calculations using density functional theory (DFT) predict an antiferromagnetic ground state with stripelike order as in the other pnictides, albeit in a shallow energy minimum compared to the nonmagnetic state.[7,8] In contrast, angle-resolved photoemission spectroscopy (ARPES) measurements report only poor nesting.[9] In fact, recent neutron scattering measurements find strong SDW fluctuations[10,11] with an incommensurate vector[11] slightly shifted from the commensurate order observed in the other iron pnictide superconductors. Also, functional renormalization group calculations[12] predict SDW fluctuations to be the dominant instability. On the other hand, recent de Haas-van Alphen (dHvA) experiments claim to be in good agreement with DFT regarding the topology of the Fermi surface.[13]

It is of particular interest to identify the role of electronic correlations in this context. Starting from band structure calculations within DFT, we include correlations at the level of the dynamical mean field theory (DMFT) and analyze their effect on the electronic structure of LiFeAs. The band structure of LiFeAs features two shallow hole pockets around the Γ point which generate a large density of states, and it has been suggested that this is essential for the way superconductivity emerges in this compound.[9,14] These features of the electronic structure can also be expected to be rather susceptible to changes induced by correlations. Thus, this paper aims to single out the effects of correlations on the Fermi surface and the low-energy properties of LiFeAs.

II. METHODS AND INTERACTION PARAMETERS

Our calculations were performed using an LDA + DMFT implementation, which combines electronic structure calculations in the full potential linearized augmented plane wave (FLAPW) framework with DMFT.[15] The electronic structure calculations were executed in WIEN2K,[16] where the self-consistency cycle employed 1080 k points in the irreducible Brillouin zone, using the local-density approximation[17] (LDA) for the exchange-correlation potential. We based our calculations on the experimental crystal structure as obtained from x-ray diffraction data[18] with space group $P\,4/nmm$. For comparison, we also performed calculations on the structure given in Ref. 2 for which we gave mass enhancements in Table I.

For the construction of localized Wannier-like orbitals for DMFT, an energy window ranging from −5.5 to 2.85 eV was chosen, comprising the Fe $3d$ and As $4p$ bands. For the solution of the DMFT impurity problem, we employed paramagnetic calculations with the strong-coupling continuous-time quantum Monte Carlo method,[19] as implemented in the ALPS code,[20,21] and considered only the density-density terms of the Hund's coupling; we used 1×10^7 Monte Carlo sweeps throughout our calculations.

For the interaction parameters, we used the definitions of $U = F^0$ and $J = (F^2 + F^4)/14$ in terms of Slater integrals[22] F^k, and the fully localized limit (FLL) double-counting correction.[23,24]

There is considerable disagreement in the literature about the size of the interaction parameters in the iron pnictides; in particular, the Coulomb interaction U strongly depends on the estimation method, whereas J is only moderately reduced from its atomic value. A self-consistent GW determination yields rather large numbers (e.g., $U = 4.9$ and $J = 0.76$ eV for $BaFe_2As_2$),[25] with lower values being reported by constrained LDA (e.g., $U = 3.1$ and $J = 0.91$ eV for LaFeAsO)[25] and constrained random-phase approximation (cRPA) (e.g., $U = 2.9$ and $J = 0.79$ eV for LaFeAsO).[15] For LiFeAs, interaction

TABLE I. Orbital-resolved quasiparticle weights Z, mass enhancements m^*/m_{LDA}, and scattering rates $-\mathrm{Im}\Sigma(i0^+)$ for interaction parameters $U = 4$ and $J = 0.8$ eV. The first (second) number in each cell refers to calculations performed on the structure from Ref. 18 (Ref. 2).

Orbital	d_{z^2}	$d_{x^2-y^2}$	d_{xy}	$d_{xz/yz}$
Z	0.57/0.53	0.64/0.60	0.36/0.31	0.42/0.36
m^*/m_{LDA}	1.74/1.88	1.57/1.67	2.78/3.24	2.39/2.78
$-\mathrm{Im}\Sigma(i0^+)$ (meV)	0.1/0.3	$-1.0/-0.7$	2.4/5.2	1.7/3.8

parameters obtained from cRPA have been reported in Ref. 26 for two low-energy models, one constructed for the Fe $3d$ bands only, and the other one for a manifold containing Fe $3d$ and As $4p$ states. The choice of the model affects the value of the interaction parameters in two ways: a model with more bands renders the associated Wannier functions more localized and thereby increases the matrix elements of the interaction. Also, since the interaction strength is derived as a partially screened Coulomb interaction where screening channels within the low-energy space are subtracted, the exclusion of more screening channels in a model with more bands increases the interactions. This is reflected by very different interaction parameters for the two models, i.e., $U = 2.45$ and $J = 0.61$ eV for the d model, and $U = 4.95$ and $J = 0.87$ eV for the dp model.

However, as pointed out in Ref. 27, the appropriate model for our LDA + DMFT approach is a hybrid model where the Wannier functions are constructed from a dp model but only d-d transitions are excluded from the screening since we only treat the d states as correlated in our DMFT procedure. This means that the d model systematically underestimates the interactions for our setup, whereas the dp model systematically overestimates them. In light of these uncertainties, we report in the following results for $U = 4$ and $J = 0.8$ eV, and include in Sec. III a discussion about the sensitivity of our results to the choice of interaction parameters.

In order to obtain real-frequency spectra from the imaginary-time Monte Carlo data, we performed analytic continuation of the self-energy using the classic maximum entropy method.[28] To avoid uncertainties from the analytic continuation, the effective masses and Fermi surfaces are directly inferred from the self-energy on the Matsubara axis: the mass enhancements read

$$m^*/m_{\mathrm{LDA}} = 1 - \left.\frac{\partial \mathrm{Im}\Sigma(i\omega)}{\partial\omega}\right|_{\omega\to 0^+}, \qquad (1)$$

where the derivative is extracted by fitting a fourth-order polynomial to the data for the lowest six Matsubara frequencies.[29] The same polynomial is used for the determination of the Fermi surfaces where we make use of the fact that the imaginary and real axis meet at zero, i.e., $\Sigma(\omega = 0) = \Sigma(i\omega = 0)$.

Calculations were performed at a temperature $T = 72.5$ K ($\beta = 160\ \mathrm{eV}^{-1}$).

In the following, orbital characters are labeled in a coordinate system which is 45° rotated with respect to the crystallographic axes, i.e., x and y point to the nearest Fe neighbors in the Fe-As plane.

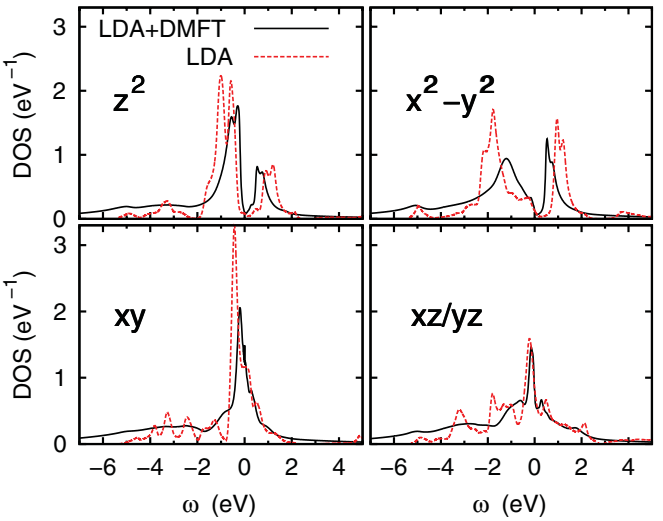

FIG. 1. (Color online) Orbital-resolved comparison between LDA density of states (red dotted lines) and the LDA + DMFT spectral function $A(\omega)$ (black solid lines). The interaction parameters used were $U = 4$ and $J = 0.8$ eV.

III. RESULTS

In Figs. 1 and 2, we compare the momentum-integrated and momentum-resolved spectral function for LiFeAs obtained within LDA + DMFT with their LDA counterparts, namely, the density of states (Fig. 1) and the LDA band energies (Fig. 2). Note that the LDA bands in Fig. 2 were renormalized by a factor of 2.17, corresponding to the orbitally averaged value of the mass renormalization.

The momentum-integrated spectral function $A(\omega)$ shows a bandwidth reduction but no substantial spectral weight transfer, i.e., no formation of Hubbard bands. The momentum-resolved spectral function $A(\mathbf{k},\omega)$ in Fig. 2 displays well-defined excitations around the Fermi level and stronger correlation-induced broadening of the states at higher binding energies. The broadening affects the states below the Fermi level more strongly where coherent quasiparticles can be identified down to approx. 0.3 eV below E_F. For the states

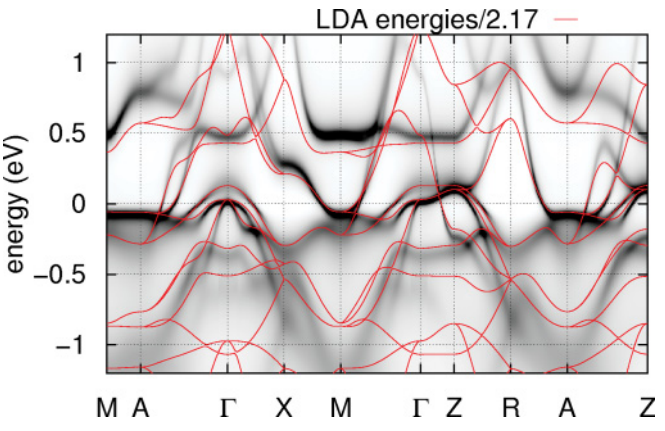

FIG. 2. (Color online) Momentum-resolved spectral function $A(\mathbf{k},\omega)$ together with LDA bands. For comparison, the LDA band energies are divided by the orbitally averaged value of the mass renormalization. The interaction parameters are the same as in Fig. 1.

above E_F, the crossover to rather diffuse structures occurs at approximately 0.7 eV. On a quantitative level, at our temperature $T = 72.5$ K, the scattering rates (or, equivalently, inverse lifetimes) $-\mathrm{Im}\Sigma(i0^+)$ are small (see Table I), supporting the picture of well-defined, long-lived quasiparticles. The renormalized LDA bands give a good approximation only close to the Fermi level [the mass enhancement in Eq. (1) holds strictly only at $\omega = 0$]; states away from E_F are less renormalized.

For the given interaction parameters, the self-energy and spectral function thus show the characteristics of a Fermi-liquid state in a metal with moderate correlations, a picture which also has been promoted for the 1111 and 122 family of iron pnictides in a number of previous publications.[15,30–33] Note that for multiorbital systems with sufficiently strong J, the absence of the rotationally invariant Hund's coupling in the calculation (i.e., the consideration of the density-density terms in J only) can lead to qualitatively wrong results by suppressing coherence and driving the system from a Fermi-liquid into a non-Fermi-liquid state.[34–36] This is not observed here, indicating that the restriction to density-density terms in the Hund's coupling is not detrimental. We also estimated the temperature below which coherent quasiparticles form by calculating $\chi(\tau = \beta/2)$, i.e., the paramagnetic local spin susceptibility at imaginary time point $\beta/2$. In a Fermi liquid, $\chi(\tau = \beta/2) \sim T^2$, and by studying the temperature dependence of $\beta^2\chi(\tau = \beta/2)$, one finds that for $U = 4$ and $J = 0.8$ eV, it takes on a constant value only at low temperatures below ≈100 K.

The mass enhancements as given in Table I exhibit pronounced orbital dependence, with stronger mass enhancement in the t_{2g} orbitals d_{xy} and d_{xz}/d_{yz}. As can also be seen from Fig. 1, the bandwidth W of the t_{2g} orbitals is smaller, leading to a larger ratio U/W and to increased correlations in these orbitals. The analysis of a low-energy iron d tight-binding model obtained by considering the localized Wannier orbitals shows that the diagonal nearest-neighbor hopping for the d_{xy} orbital, $t_{\mathrm{NN}}(xy,xy)$, almost vanishes as the direct hopping from the iron-iron overlap and the indirect hopping from the iron-pnictogen-iron overlap have opposite signs and almost cancel. Also, the diagonal hoppings to further iron neighbors for d_{xy} are small; this contributes to the localization of the d_{xy} quasiparticles and a stronger mass enhancement than in the other orbitals.[37] The table lists the mass enhancements for both investigated structures, which show some quantitative yet not qualitative differences. We checked that, in particular, Fermi

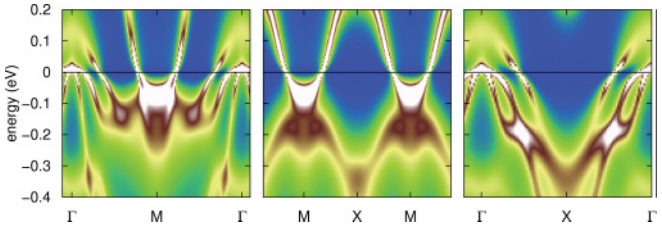

FIG. 3. (Color online) LDA+DMFT momentum-resolved spectral function $A(\boldsymbol{k},\omega)$ for LiFeAs along the paths in the Brillouin zone given in Fig. 2(e) of Ref. 9. Intensity ranges from white (maximal) to blue (minimal). Interaction parameters are as in Fig. 1.

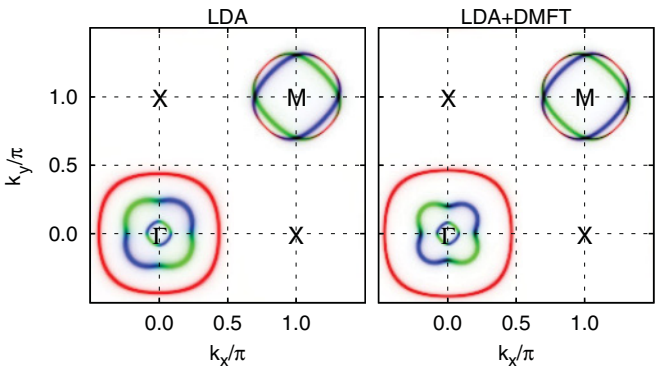

FIG. 4. (Color online) Fermi surface for $k_z = 0$. Color code for orbital characters: d_{xy} (red), d_{xz} (green), and d_{yz} (blue). Interaction parameters are as in Fig. 1.

surfaces are practically not affected, though; we therefore continue to give results only for the structure from Ref. 18.

For a comparison with ARPES measurements, Fig. 3 shows some cuts of the momentum-resolved spectral function $A(\boldsymbol{k},\omega)$ along the paths given in Fig. 2(e) in Ref. 9. Qualitatively, we find good agreement; quantitatively, the mass enhancement extracted from these cuts in Ref. 9 is 3.1. This value should be compared to the mass enhancements of the orbitals that contribute most to the spectral weight at low energy. As can be seen from Fig. 1, these are the t_{2g} orbitals (the e_g orbitals show a dip around the Fermi level) with calculated mass enhancements of 2.4–2.8 (2.8–3.2, respectively). Thus, mass enhancements are in good agreement, with ARPES pointing to moderately larger interactions. We will come back to this point further below.

In summary, we consider LiFeAs to be a metal in an intermediate range of interactions without significant spectral weight transfer. Mass renormalizations are close to what has been calculated and measured in the 1111 and 122 systems; compared to, e.g., LaFeAsO,[38] coherent quasiparticles seem to form at lower temperatures, with the spin susceptibility approaching Fermi-liquid-like behavior only below ≈100 K.

We now turn our attention to the discussion of the effects of correlations on the Fermi surfaces of LiFeAs, which have been experimentally accessed by ARPES and dHvA[13] measurements. Figures 4 and 5 show the Fermi surfaces in the $k_z = 0$ and $k_z = \pi$ plane obtained within LDA and LDA +

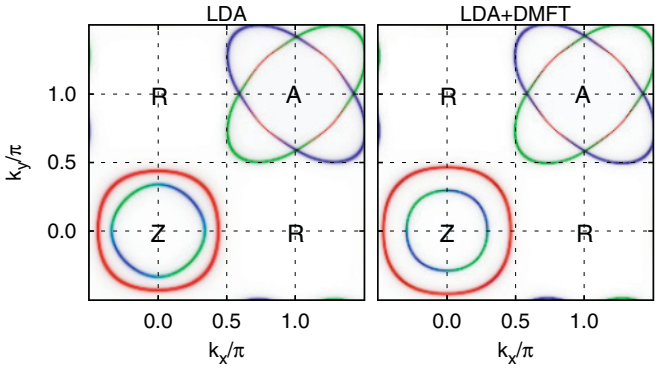

FIG. 5. (Color online) Fermi surface for $k_z = \pi$. Color code and interaction parameters are as in Fig. 4.

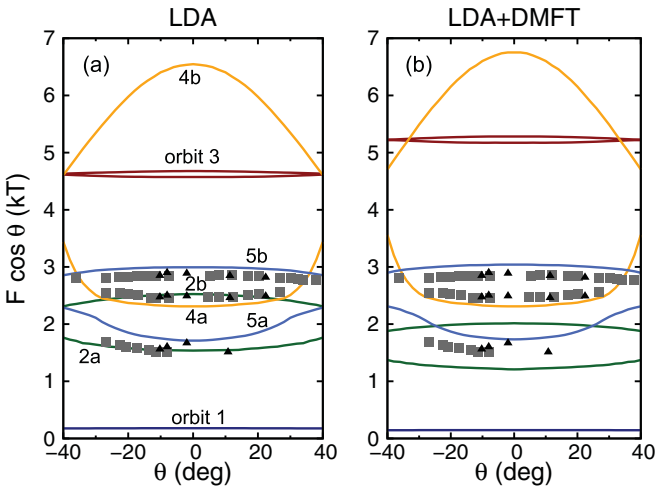

FIG. 6. (Color online) dHvA frequencies with respect to magnetic field angle obtained within (a) LDA and (b) LDA+DMFT. The orbits refer to extremal pocket sizes where the pockets are identified as discussed in the text. Interaction parameters are as in Fig. 1. Triangles (pulsed field) and squares (dc field) are experimental data taken from Ref. 13.

DMFT. The pockets around $(k_x,k_y) = (0,0)$ are hole pockets, while the ones around $(k_x,k_y) = (\pi,\pi)$ are electron pockets (compare Fig. 2). The most prominent effects of correlations are the shrinking of the middle d_{xz}/d_{yz} hole pocket, which takes on a butterfly shape at $k_z = 0$, and the increase of the outer d_{xy} pocket, whereas the electron pockets almost do not change in size or form. This observation is in agreement with previous calculations[37] and would support ARPES results. This analysis shows that correlations tend to weaken—if not suppress—nesting in this material.

For the discussion of the electron pockets, we describe the Fermi surface in terms of an inner and outer pocket rather than by two crossed ellipse-like pockets of equal size. This is motivated by the fact that spin-orbit (SO) coupling lifts the degeneracy between the ellipses and splits the electron pockets into an inner and outer sheet.[13,39,40] Note, however, that no SO coupling is taken into account in the present calculation. As one can see from the comparison of Figs. 4 and 5, the thus defined outer pocket has strong k_z dispersion, whereas the inner sheet depends only weakly on k_z.

In order to facilitate a quantitative comparison with the dHvA measurements, we show in Fig. 6 calculated dHvA frequencies with respect to magnetic field angle, as reported in Fig. 2(c) of Ref. 13. The dHvA frequencies correspond to extremal pocket sizes (orbits) that are observed at a given angle θ with respect to the k_z axis. The labeling of the orbits follows Ref. 13: orbits 1, 2, and 3 refer to the inner, middle, and outer hole pocket, and orbits 4 and 5 refer to the outer and inner electron pocket [see Fig. 6(a)]. In order to define pocket sizes within LDA + DMFT [Fig. 6(b)] in view of the finite broadening induced by the correlations, we track the maximum of $A(\omega = 0)$ through the Brillouin zone.

Compared to the calculated dHvA frequencies in Ref. 13, small differences are already visible on the LDA level [Fig. 6(a)], e.g., the minima of orbit 2 and orbit 5 for small angles are not degenerate anymore. This is probably an effect of differences in the determination of the Fermi surface (e.g., due to effects of a finite k-mesh) and illustrates the high sensitivity of the orbits to details of the calculation.

As already seen in Figs. 4 and 5, the effect of correlations on the Fermi surface manifests itself mainly in a shrinking of the middle hole pocket, and, in order to preserve the electron count, an increase of the outer hole pocket size. This is reflected merely by a shift downward of orbit 2 and a shift upward of orbit 3 in Fig. 6(b); a change in the warping would indicate a change in the k_z structure of the pocket, which is not to be expected from the local, i.e., k-independent, interaction in (single-site) DMFT.

Analyzing the curvature and the size of the orbits, the authors of Ref. 13 attribute the experimentally measured frequencies to the electron Fermi surface sheets, where the two higher frequencies are assigned to orbits 5b and 4a, and the lowest frequency is suspected to originate from orbit 5a.[40] Our results support this interpretation: whereas the orbits 2a/5a and 2b/4a are of similar size in the LDA calculation, the correlations affect mainly the hole pockets and lift this (near) degeneracy. As a result, the electron orbits 2a and 2b are unlikely to give rise to the measured frequencies, as their sizes are rather different from the measured data. This offers a reconciliation of the dHvA and ARPES experiments: the shrunk middle hole pocket is only seen in ARPES, which finds a correlated metal with poor nesting together with sizable mass renormalization. In contrast, the dHvA measurements resolve the (lighter) electron pocket sizes in LiFeAs that almost do not change under inclusion of correlation, and therefore report good agreement with LDA. The large mass renormalizations (up to $\approx$5) that are also measured in Ref. 13 suggest—even under consideration of a non-negligible electron-phonon contribution—a scenario of important electronic correlations which are correctly accounted for within LDA + DMFT.

In LiFeP, which was also investigated in the same work,[13] the situation is different. Whereas the middle hole pocket in LiFeAs is particulary shallow with a band energy of 64 meV above E_F at the Γ point, the pocket in LiFeP is roughly of the same size as in LiFeAs; however, the corresponding band energy at Γ is 155 meV. Hence, the dispersion in LiFeP is considerably stronger, rendering the pocket less susceptible to band shifts as induced by the real part of the self-energy, i.e., less susceptible to correlations. Consequently, the dHvA frequencies remain rather unchanged upon the inclusion of correlations.

A. Sensitivity to interaction parameters

We analyze the sensitivity of our results to our choice of interaction parameters by applying some variation to U and J, while keeping the respective other parameter fixed.

Figure 7 shows the evolution of the mass enhancements m^*/m_{LDA} with the interaction parameters. A moderate dependence on U and a very strong dependence on J are observed (note that the applied variations of U and J are different in size). Whereas a change in U affects all orbitals roughly equally, a change in J leads to an immense mass enhancement, particulary of the t_{2g} orbitals.

The decisive role of the Hund's coupling for the physical properties of the iron pnictides has been discussed

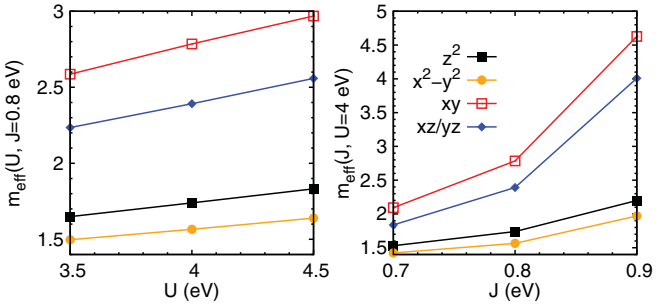

FIG. 7. (Color online) Sensitivity of effective masses m^*/m_{LDA} with respect to changes in the interaction parameters.

previously.[34] For the different behavior of the e_g and t_{2g} orbitals, it is important that the e_g states in LiFeAs lie energetically lower than the t_{2g} states. In the atomic limit, the energy gain from Hund's rule exceeds the crystal-field splitting already for rather small J, and the ground state is a high spin state with the configuration $e_g^3 t_{2g}^3$, where the t_{2g} orbitals are occupied by three electrons of the same spin. In the atomic limit, this prevents mixing of the orbitals due to the Pauli principle; in the crystal, it still impedes interorbital fluctuations within the t_{2g} manifold.[37,41] This effect contributes to the high sensitivity of the t_{2g} effective masses with respect to J.

Accordingly, the Fermi surface is rather stable against variation of U, but strongly depends on J, as shown for $k_z = 0$ in Fig. 8 and $k_z = \pi$ in Fig. 9. Following the trend discussed above, larger values of J promote a more pronounced shrinking (increase) of the middle (outer) hole pocket. Values as large as 0.9 eV for the Hund's coupling render the system rather incoherent, with significant scattering

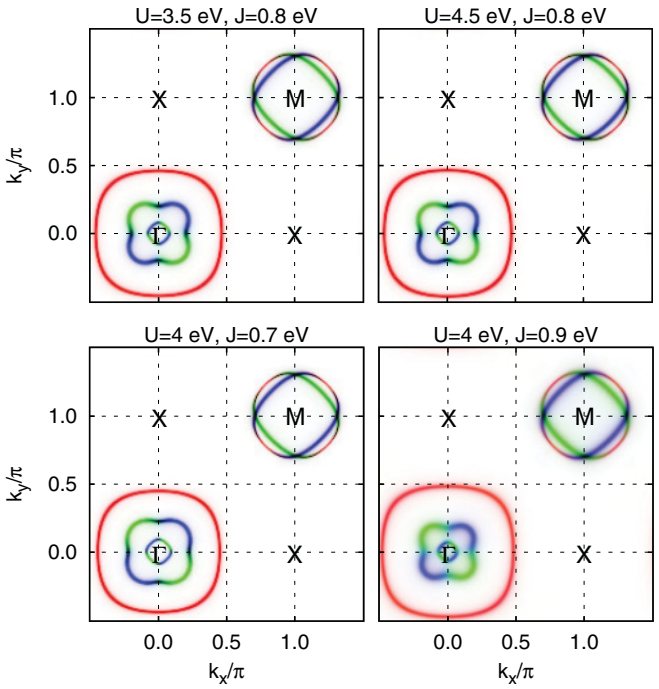

FIG. 8. (Color online) Sensitivity of the Fermi surface at $k_z = 0$ with respect to changes in the interaction parameters.

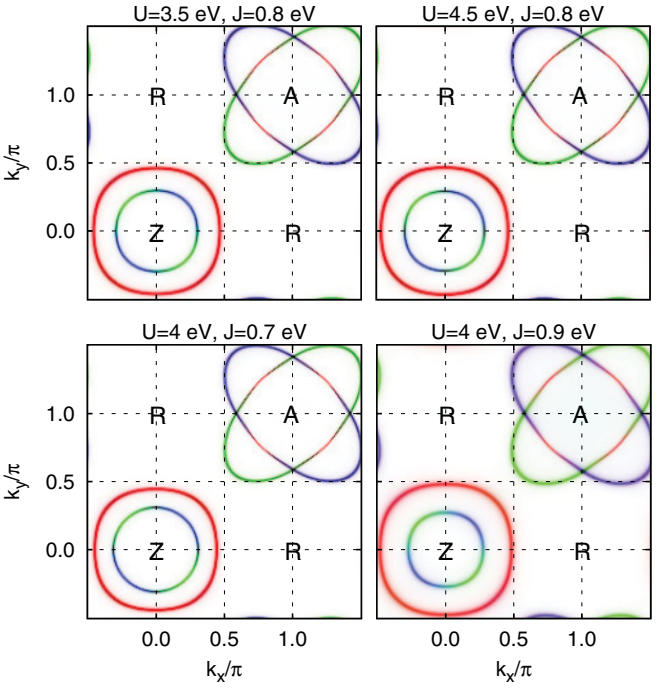

FIG. 9. (Color online) Sensitivity of the Fermi surface at $k_z = \pi$ with respect to changes in the interaction parameters.

rates $-\mathrm{Im}\Sigma(i0^+)$ around 14 meV on the t_{2g} orbitals. This causes the broadening of the respective Fermi surface in Figs. 8 and 9. Future calculations with the full Hund's rule coupling are required to check whether the occurrence of the coherence-incoherence crossover already at $J \lesssim 0.9$ eV is a physical effect or an artifact of the breaking of the rotational invariance by density-density interactions.

IV. CONCLUSIONS

We showed that within the considered range of interaction parameters, LiFeAs behaves as a Fermi liquid where correlation effects are very sensitive to the value of the Hund's rule coupling, particularly for the t_{2g} orbitals. The strong mass enhancements measured in both ARPES and dHvA experiments suggest sizable correlations of the size considered in this work. While electron-phonon effects have been reported[42] to be significant and contribute to the slightly higher mass enhancements measured experimentally, they cannot account alone for the large values observed. As for the Fermi surface, the correlations mainly affect the hole pockets that significantly change in size. We propose this as the source of the seeming discrepancy of the ARPES and dHvA experiments: whereas dHvA presumably observes only electron orbits with sizes close to their LDA values, ARPES finds the reduced size of the middle hole pocket as the most prominent feature. In this way, the two experiments can be reconciled. The selective size reduction of the middle hole pocket also renders nesting less efficient.

ACKNOWLEDGMENTS

We would like to thank C. Putzke, B. Büchner, and especially A. Coldea and M. Aichhorn for very useful

discussions. We gratefully acknowledge financial support from the Deutsche Forschungsgemeinschaft through Program No. SPP 1458 and from the Helmholtz Association through Grant No. HA216/EMMI.

*ferber@itp.uni-frankfurt.de

[1] D. C. Johnston, Adv. Phys. **59**, 803 (2010).
[2] J. H. Tapp, Z. Tang, B. Lv, K. Sasmal, B. Lorenz, P. C. W. Chu, and A. M. Guloy, Phys. Rev. B **78**, 060505 (2008).
[3] M. J. Pitcher, D. R. Parker, P. Adamson, S. J. C. Herkelrath, A. T. Boothroyd, R. M. Ibberson, M. Brunelli, and S. J. Clarke, Chem. Commun. **45**, 5918 (2008).
[4] Z. Deng, X. C. Wang, Q. Q. Liu, S. J. Zhang, Y. X. Lv, J. L. Zhu, R. C. Yu, and C. Q. Jin, Europhys. Lett. **87**, 37004 (2009).
[5] Y. Kamihara, H. Hiramatsu, M. Hirano, R. Kawamura, H. Yanagi, T. Kamiya, and H. Hosono, J. Am. Chem. Soc. **128**, 10012 (2006).
[6] D. J. Singh, Physica C **469**, 418(2009).
[7] D. J. Singh, Phys. Rev. B **78**, 094511 (2008).
[8] Y.-Z. Zhang, I. Opahle, H. O. Jeschke, and R. Valentí, Phys. Rev. B **81**, 094505 (2010).
[9] S. V. Borisenko, V. B. Zabolotnyy, D. V. Evtushinsky, T. K. Kim, I. V. Morozov, A. N. Yaresko, A. A. Kordyuk, G. Behr, A. Vasiliev, R. Follath, and B. Büchner, Phys. Rev. Lett. **105**, 067002 (2010).
[10] A. E. Taylor, M. J. Pitcher, R. A. Ewings, T. G. Perring, S. J. Clarke, and A. T. Boothroyd, Phys. Rev. B **83**, 220514(R) (2011).
[11] N. Qureshi, P. Steffens, Y. Drees, A. C. Komarek, D. Lamago, Y. Sidis, L. Harnagea, H. J. Grafe, S. Wurmehl, B. Büchner, and M. Braden, e-print arXiv:1108.6187 (Phys. Rev. Lett., in press).
[12] C. Platt, R. Thomale, and W. Hanke, Phys. Rev. B **84**, 235121 (2011).
[13] C. Putzke, A. I. Coldea, I. Guillamón, D. Vignolles, A. McCollam, D. LeBoeuf, M. D. Watson, I. I. Mazin, S. Kasahara, T. Terashima, T. Shibauchi, Y. Matsuda, and A. Carrington, Phys. Rev. Lett. **108**, 047002 (2012).
[14] P. M. R. Brydon, M. Daghofer, C. Timm, and J. van den Brink, Phys. Rev. B **83**, 060501(R) (2011).
[15] M. Aichhorn, L. Pourovskii, V. Vildosola, M. Ferrero, O. Parcollet, T. Miyake, A. Georges, and S. Biermann, Phys. Rev. B **80**, 085101 (2009).
[16] P. Blaha, K. Schwarz, G. K. H. Madsen, D. Kvasnicka, and J. Luitz, computer code WIEN2K (Technische Universität Wien, Austria, 2001).
[17] J. P. Perdew and Y. Wang, Phys. Rev. B **45**, 13244 (1992).
[18] I. Morozov, A. Boltalin, O. Volkova, A. Vasiliev, O. Kataeva, U. Stockert, M. Abdel-Hafiez, D. Bombor, A. Bachmann, L. Harnagea, M. Fuchs, H.-J. Grafe, G. Behr, R. Klingeler, S. Borisenko, C. Hess, S. Wurmehl, and B. Büchner, Cryst. Growth Design **10**, 4428 (2010).
[19] P. Werner, A. Comanac, L. de' Medici, M. Troyer, and A. J. Millis, Phys. Rev. Lett. **97**, 076405 (2006).
[20] B. Bauer, L. D. Carr, H. G. Evertz, A. Feiguin, J. Freire, S. Fuchs, L. Gamper, J. Gukelberger, E. Gull, S. Guertler, A. Hehn, R. Igarashi, S. V. Isakov, D. Koop, P. N. Ma, P. Mates, H. Matsuo, O. Parcollet, G. Pawłowski, J. D. Picon, L. Pollet, E. Santos, V. W. Scarola, U. Schollwöck, C. Silva, B. Surer, S. Todo, S. Trebst, M. Troyer, M. L. Wall, P. Werner, and S. Wessel, J. Stat. Mech. (2011) P05001.
[21] E. Gull, P. Werner, S. Fuchs, B. Surer, T. Pruschke, and M. Troyer, Comp. Phys. Commun. **182**, 1078 (2011).
[22] V. I. Anisimov, F. Aryasetiawan, and A. I. Lichtenstein, J. Phys. Condens. Matter **9**, 767 (1997).
[23] V. I. Anisimov, I. V. Solovyev, M. A. Korotin, M. T. Czyżyk, and G. A. Sawatzky, Phys. Rev. B **48**, 16929 (1993).
[24] S. L. Dudarev, G. A. Botton, S. Y. Savrasov, C. J. Humphreys, and A. P. Sutton, Phys. Rev. B **57**, 1505 (1998).
[25] A. Kutepov, K. Haule, S. Y. Savrasov, and G. Kotliar, Phys. Rev. B **82**, 045105 (2010).
[26] T. Miyake, K. Nakamura, R. Arita, and M. Imada, J. Phys. Soc. Jpn. **79**, 044705 (2010).
[27] T. Miyake, L. Pourovskii, V. Vildosola, S. Biermann, and A. Georges, J. Phys. Soc. Jpn. **77**, 99 (2008).
[28] M. Jarrell and J. E. Gubernatis, Phys. Rep. **269**, 133 (1996).
[29] J. Mravlje, M. Aichhorn, T. Miyake, K. Haule, G. Kotliar, and A. Georges, Phys. Rev. Lett. **106**, 096401 (2011).
[30] V. I. Anisimov, D. M. Korotin, M. A. Korotin, A. V. Kozhevnikov, J. Kuneš, A. O. Shorikov, S. L. Skornyakov, and S. V. Streltsov, J. Phys. Condens. Matter **21**, 075602 (2009).
[31] S. L. Skornyakov, A. V. Efremov, N. A. Skorikov, M. A. Korotin, Y. A. Izyumov, V. I. Anisimov, A. V. Kozhevnikov, and D. Vollhardt, Phys. Rev. B **80**, 092501 (2009).
[32] S. L. Skornyakov, N. A. Skorikov, A. V. Lukoyanov, A. O. Shorikov, and V. I. Anisimov, Phys. Rev. B **81**, 174522 (2010).
[33] P. Hansmann, R. Arita, A. Toschi, S. Sakai, G. Sangiovanni, and K. Held, Phys. Rev. Lett. **104**, 197002 (2010).
[34] K. Haule and G. Kotliar, New J. Phys. **11**, 025021 (2009).
[35] H. Ishida and A. Liebsch, Phys. Rev. B **81**, 054513 (2010).
[36] M. Aichhorn, S. Biermann, T. Miyake, A. Georges, and M. Imada, Phys. Rev. B **82**, 064504 (2010).
[37] Z. P. Yin, K. Haule, and G. Kotliar, Nat. Mater. **10**, 932 (2011).
[38] M. Aichhorn, L. Pourovskii, and A. Georges, Phys. Rev. B **84**, 054529 (2011).
[39] We performed fully relativistic calculations [43] of the Fermi surface of LiFeAs to confirm the avoided crossing of the electron sheets.
[40] A. Coldea (private communication).
[41] L. de' Medici, Phys. Rev. B **83**, 205112 (2011).
[42] A. A. Kordyuk, V. B. Zabolotnyy, D. V. Evtushinsky, T. K. Kim, I. V. Morozov, M. L. Kulić, R. Follath, G. Behr, B. Büchner, and S. V. Borisenko, Phys. Rev. B **83**, 134513 (2011).
[43] K. Koepernik and H. Eschrig, Phys. Rev. B **59**, 1743 (1999); [http://www.FPLO.de].